ACCSCIENCE PUBLISHING

International Journal of Bioprinting

RESEARCH ARTICLE

PBF-LB fabrication of microgrooves for induction of osteogenic differentiation of human mesenchymal stem cells

Aira Matsugaki*, Tadaaki Matsuzaka, Toko Mori, Mitsuka Saito, Kazuma Funaoku, Riku Yamano, Ozkan Gokcekaya, Ryosuke Ozasa, and Takayoshi Nakano*

Division of Materials and Manufacturing Science, Graduate School of Engineering, Osaka University, 2-1 Yamada-oka, Suita, Osaka 565-0871, Japan

Abstract

Stem cell differentiation has important implications for biomedical device design and tissue engineering. Recently, inherent material properties, including surface chemistry, stiffness, and topography, have been found to influence stem cell fate. Among these, surface topography is a key regulator of stem cells in contact with materials. The most important aspect of ideal bone tissue engineering is to control the organization of the bone extracellular matrix with fully differentiated osteoblasts. Here, we found that laser powder bed fusion (PBF-LB)-fabricated grooved surface inspired by the microstructure of bone, which induced human mesenchymal stem cell (hMSC) differentiation into the osteogenic lineage without any differentiation supplements. The periodic grooved structure was fabricated by PBF-LB which induced cell elongation facilitated by cytoskeletal tension along the grooves. This resulted in the upregulation of osteogenesis via *Runx2* expression. The aligned hMSCs successfully differentiated into osteoblasts and further organized the bone mimetic-oriented extracellular matrix microstructure. Our results indicate that metal additive manufacturing technology has a great advantage in controlling stem cell fate into the osteogenic lineage, and in the construction of bone-mimetic microstructural organization. Our findings on material-induced stem cell differentiation under standard cell culture conditions open new avenues for the development of medical devices that realize the desired tissue regeneration mediated by regulated stem cell functions.

Keywords: Additive manufacturing; Laser powder bed fusion; Mesenchymal stem cells; Osteogenic differentiation; Bone microstructure

***Corresponding authors:**
Takayoshi Nakano
(nakano@mat.eng.osaka-u.ac.jp)

Aira Matsugaki
(matsugaki@mat.eng.osaka-u.ac.jp)

Citation: Matsugaki A, Matsuzaka T, Mori T, et al. PBF-LB fabrication of microgrooves for induction of osteogenic differentiation of human mesenchymal stem cells. *Int J Bioprint*. 2024;10(1):1425. doi: 10.36922/ijb.1425

Received: December 30, 2022
Accepted: August 8, 2023
Published Online: January 9, 2024

1. Introduction

Mesenchymal stem cells (MSCs) are multipotent cells that can differentiate into various tissues, including bone, fat, cartilage, muscle, and neurons.[1] Osteogenic differentiation of MSCs has been of interest for use as an autologous cell source, or for the development of medical devices in bone engineering.[2,3] Tailored control of human mesenchymal stem cells (hMSCs) differentiation is desirable in biomedical engineering and stem cell

biology. The putative factors that play key roles in stem cell differentiation have been believed biochemical molecules, including growth factors and biological supplements.

However, it is increasingly recognized that environmental cues can determine cell fate specifications.[4] Limited reports have shown that stem cell lineage can be controlled using only inherent material properties. For example, scaffold mechanical stiffness,[5,6] surface topography,[7,8] and materials degradation[9,10] have been reported to impact stem cell fate. Topographical control of somatic cells has been developed over decades and is associated with nanotechnological advances.[11-13] Metal additive manufacturing is a powerful tool for providing the desired material properties through three-dimensional (3D) structural design.[14,15] This technique realizes the fabrication of required structure with particular shape and porosity from micrometer-sized metal powders, which serve as the starting materials. Focusing on the microstructure of intact bone tissue, orderly-shaped materials mimicking the bone matrix structure have serious advantages for guiding functional bone regeneration.[16-19] Living bone tissue exhibits high-strength mechanical characteristics in the required direction because of preferred collagen elongation and apatite crystal formation.[20] The crystallographic anisotropy of bone varies significantly depending on the anatomical portion.[21] However, it is difficult to spontaneously reconstruct bone matrix microstructure in regenerated or diseased bones that have lost their appropriate organized matrix, even if the bone density is satisfactorily recovered.[22] Artificial control of the ordered osteoblast alignment provides an oriented microstructure for bone matrix formation, which directs the requisite mechanical properties. Molecular interactions between cells and materials play key roles in the organization of the bone matrix.[23] The key to recovering lost bone function is the reconstruction of the bone-mimetic anisotropic microstructure with fully differentiated osteoblasts. Additive manufacturing control of a parallel groove structure is proposed here to control stem cell alignment as well as differentiation behaviors. The laser powder bed fusion (PBF-LB) method, a type of metal additive manufacturing, enables elaborate 3D structural control. PBF-LB is a powerful next-generation technology, and it fulfills the goal of using biomimetic materials to create artificial organs. Indeed, our recent research developed an additive-manufactured vertebral fusion cage device that can induce significantly superior bone fusion without utilizing a large amount of autologous bone.[24,25]

In this study, artificial control of the hMSCs differentiation lineage was achieved using a scaffold surface structure, without any differentiation stimuli. The additive-manufactured groove structure fulfilled the requirements for osteogenic differentiation of hMSCs, in association with unidirectional bone matrix organization.

2. Materials and methods

2.1. Fabrication of substrates by metal additive manufacturing

The substrates were fabricated from Ti-6Al-4V powder using PBF-LB based on the computer-aided design (CAD) data. The substrates were then acid-cleaned with nitric hydrofluoric acid to remove molding defects that occur during the layered molding process. After acid cleaning was completed, the substrate was degreased, and impurities were removed from the surface by ultrasonic cleaning. The substrates were sterilized (121°C, 20 min) in an autoclave (Series 540, NAPCO) for use in cell culture tests.

2.2. Analysis of substrate surface topography

A confocal laser microscope (VK-9700, Keyence, Osaka, Japan) was used to quantitatively evaluate the surface topography of the substrates. Line profiles were acquired per field of view, and the peak width and height were measured for each profile. For the control substrate, the surface roughness (Sa; arithmetical mean height), which means area roughness, was measured. In addition, the surface topography of the substrate was observed by field-emission scanning electron microscopy (FE-SEM; JIB-4610F, JEOL, Japan) operated at 20 kV and 16 mA. Substrates were washed with acid for a short time, followed by acetone, ethanol, and water, before observation.

2.3. Mesenchymal stem cell culture

Human mesenchymal stem cells from bone marrow (Takara Bio Inc., Shiga, Japan) were seeded at a concentration of 5000 cells/cm^2 in MSC culture medium (Mesenchymal Stem Cell Growth Medium 2 [Takara] mixed with SupplementMix MSC Growth Medium 2 [Takara], Penicillin Streptomycin [Gibco, Carlsbad, CA, USA]). The cells were cultured at 37°C and 5.0% CO_2. Cells were cultured for 1 day in short-term culture and 4 weeks in long-term culture. In both short- and long-term cultures, the medium was replaced twice a week. All operations were performed in a safety cabinet to prevent bacterial contamination.

2.4. Immunofluorescent staining

Mesenchymal stem cells were fixed by replacing the culture medium with 4% formalin/phosphate-buffered saline (PBS) and allowed to stand for 20 min. The cells were then washed twice with PBST (PBS 0.05% TritonX) for 10 min each time. The non-specific signals were blocked with 5% normal goat serum (Invitrogen, Carlsbad, CA, USA) for 30 min and then replaced with the primary antibody solution at 4°C overnight. The cells were washed and then incubated

with a secondary antibody and Hoechst staining The aforementioned as well as subsequent manipulations were performed while keeping the cells away from light. The cells were then washed thrice for 10 min each time in PBST and incubated in PBST containing phalloidin (Invitrogen, Carlsbad, CA, USA). After that, the stained samples were mounted in ProLong™ Gold Antifade Mountant (Thermo Fisher Scientific, Carlsbad, CA, USA).

2.5. Cell orientation analysis

Immunofluorescence staining was performed to quantitatively analyze the morphological changes in MSCs on culture substrates. For each sample, images of F-actin, vinculin, and nuclei were taken at multiple points with a 20× objective lens using a fluorescence microscope (BZ-X710, Keyence). Images were captured by focusing on cells adhering from the top of the groove shape. Single cells were analyzed, excluding those whose cell morphology was difficult to accurately distinguish, and 40–60 stained cells were analyzed per sample. Images of the nuclei and F-actin/vinculin-stained images were gray scaled using Photoshop 6.0 (Adobe Inc., Mountain View, CA, USA) and further binarized. Both images were loaded into CellProfiler (Broad Institute Cambridge, MA, USA) to recognize the shape of the cell body based on the position of the cell nucleus. The cell shape was approximated as an ellipse. The angle between the major axis of the ellipse and the groove direction on the substrate was defined as 0, and was represented in a histogram at 10° intervals. To designate the flat substrate, is the angle between the major axis of the ellipse and the scanning direction during modeling. The degree of cell orientation was defined as a value representing the degree of cell orientation using the following equation[26]:

$$R = 2\left(\left\langle cos^2\theta_k \right\rangle - \frac{1}{2} \right) \quad \text{(I)}$$

$$\left\langle \cos^2 \theta_k \right\rangle = \frac{\left(\sum_1^n \cos^2 \theta_k \right)}{n} \quad \text{(II)}$$

Under this definition, R=1 when all cells are aligned perfectly parallel to the groove direction (θk = 0°); conversely, R = 0 when perfectly unoriented (θk… at random).

2.6. Single-cell RNA sequencing

The culture medium was removed, and the cells were washed twice with PBS. Then, 250 μL of each of the cell detachment agents (accutase: collagenase = 3:2) was injected and kept in the incubator for 10 min. Mesenchymal stem cells were then filtered through a cell strainer to obtain single cells. After centrifugation, the supernatant was removed, and 1 mL of PBS was added to the suspension. The cell concentration was adjusted to 2 × 10^5 cells/mL in PBS. After that, the sample cell mixture for ICELL8 cx aliquot was prepared.

The recovered cDNA was enriched using the DNA Clean & 5-kit (Zymo Research). To the cDNA product, 0.6× volume of AMPure XP beads was added, mixed by pipetting, and incubated at room temperature for 5 min. They were then placed on a magnetic stand and allowed to stand for 2 min. The supernatant was removed with a pipette, and 200 μL of 70% ethanol was added to wash the beads and allowed to stand for 1 min. The tube was then rotated and allowed to stand for 10 s on one side of the tube, and then reversed and allowed to stand again for 10 s on the other side. This procedure was repeated twice, and then the supernatant was removed with a pipette, and the procedure was repeated twice. Subsequently, the ethanol was removed with the tube still in place, the lid was opened, and the beads were allowed to stand for less than 2 min to dry. Next, 13 μL of DNase-RNase-free water was added, mixed by pipetting, and incubated for 5 min. After allowing it to stand for 1 min, 12 μL of the supernatant was collected and transferred to a new tube. The resulting cDNA was quantified using the Qubit dsDNA HS Assay Kit (Life Technologies), and a Qubit 3.0 Fluorometer, High Sensitivity DNA Kit, and Agilent 2100 Bioanalyzer were used to confirm the quality of the cDNA libraries. Library length was measured and quantified using a High Sensitive DNA Kit and Agilent 2100 Bioanalyzer for sequence analysis. The library was sequenced using the HiSeq2500 for Read1:26 cycles and Read2:101 cycles, and approximately 250 million reads were obtained.

2.7. Alkaline phosphatase assay

To verify osteogenic differentiation, alkaline phosphatase activity was measured using the Alkaline Phosphatase Colorimetric Assay Kit (Abcam) according to the manufacturer's protocols. Cells were exposed to the culture medium for 3 days, after which samples were washed twice with PBS. Then, 50 μL of cell lysate with assay buffer was added to a 96-well plate, and 50 μL of p-nitrophenyl phosphate was added. Samples were light-shielded and incubated at 25°C for 60 min. Finally, 20 μL of stop solution was added to the wells, and the absorbance was analyzed at 405 nm and measured at 650 nm as a reference (MULTICKAN FC, Thermo Fisher Scientific).

2.8. Statistical analysis

The data obtained from the experiments are expressed as the mean ± SD. Student's *t*-test was used for comparisons between two groups, and Tukey's test was used for comparisons among three or more groups. A difference was considered significant if the *p*-value was less than 0.05

for both tests. The sample sizes for cell analysis and single-cell RNA sequencing were 5 and 3, respectively.

3. Results

3.1. Surface topography of the 3D-printed Ti-6Al-4V surface

The 3D profile of each metal-printed substrate surface was obtained using a laser microscope (Figure 1). In addition to the surface roughness (Sa) obtained from the 3D profiles, the peak widths and heights measured from the line profiles for each of these surfaces are summarized. The peak heights of 1000, 500, and 250 μm substrates deviated from the designed value (100 μm) and the measured values. On the other hand, groove widths with the same measured values as the design values were obtained with good accuracy. The surface roughness values showed no significant differences among the groups.

3.2. Quantitative analysis of mesenchymal stem cell orientation

Although MSCs on the control flat showed cell elongation, the average angle of cell orientation showed no preferred direction (Figure 2A). In contrast, MSCs on all substrates with groove structures of 1000 μm or less tended to elongate preferentially in the direction of the grooves. The results of the quantitative analysis of the cell orientation in each group showed that the narrower the groove width of the metal printing substrate, the higher the degree of cell orientation (Figure 2B). Furthermore, the cells were distributed in ridges, indicating that the adhesion spots were favored to locate on the slopes in periodic microstructure (Figure 2C and D). In particular, cells on the 100 μm substrate showed characteristic adhesion limited at the slopes.

3.3. Gene expression analysis by single-cell RNA sequencing

Stemness properties of the cultured hMSCs were analyzed by the comparison of *CD90*, *CD44,* and *SH2* expression analysis. The expression of *CD90*, a known stem cell marker of MSC, was significantly decreased in MSCs cultured on 100 μm substrate, as well as the decreasing tendency in expression was also noted in *CD44* and *SH2* (Figure 3A). We also examined the differentiation marker genes expressed when MSCs differentiated into other cell types. The ratio of the number of cells expressing the five marker genes, *Runx2* (osteoblast marker gene), *PPARγ* (adipocyte marker gene), *Sox9* (chondrocyte marker gene), *Tuj1* (nerve cell marker gene), and *MyoD1* (muscle cell marker gene), to the total number of cells is shown in Figure 3B. The ratio of the number of cells expressing the five marker genes was compared with the total number of cells expressing the genes. The number of cells expressing *Sox9, MyoD1*, and *Tuj1* was very low (less than 5%), whereas the number of cells expressing *Runx2* and *PPARγ* was higher than that of the other three factors. Figure 3C shows the number and distribution of the cells expressing these two genes under each condition. *PPARγ* showed almost the same level of expression, but the expression level of *Runx2* showed a tendency to increase in the grooved substrate. Furthermore, ALP activation was significantly increased on the 100 μm groove substrate compared to that on the control (Figure 3D). Immunocytochemical analysis showed high expression of *Runx2* in cells aligned along the grooves (Figure 3E). Quantitative cell deformation analysis demonstrated that the oriented cells showed elongation with a high aspect ratio along the direction of the grooves (Figure 3F).

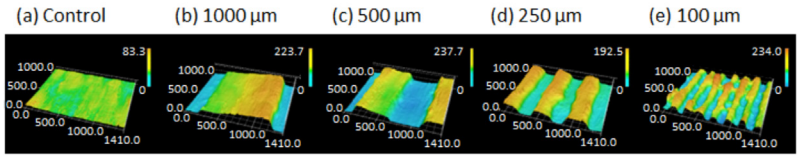

	(a) Control	(b) 1000 μm	(c) 500 μm	(d) 250 μm	(e) 100 μm
Roughness (Sa) [μm]					
	0.85 ± 0.23	0.59 ± 0.18	0.71 ± 0.33	0.78 ± 0.37	0.68 ± 0.32
Width [μm]					
	—	998.87 ± 27.28	516.49 ± 14.60	250.02 ± 20.88	112.56 ± 29.74
Depth [μm]					
	—	211.75 ± 17.75	168.89 ± 12.59	142.53 ± 19.09	117.18 ± 26.53

Figure 1. Surface characterization of additive-manufactured grooved substrates: (a) control (without grooves), (b) 1000 μm, (c) 500 μm, (d) 250 μm, and (e) 100 μm.

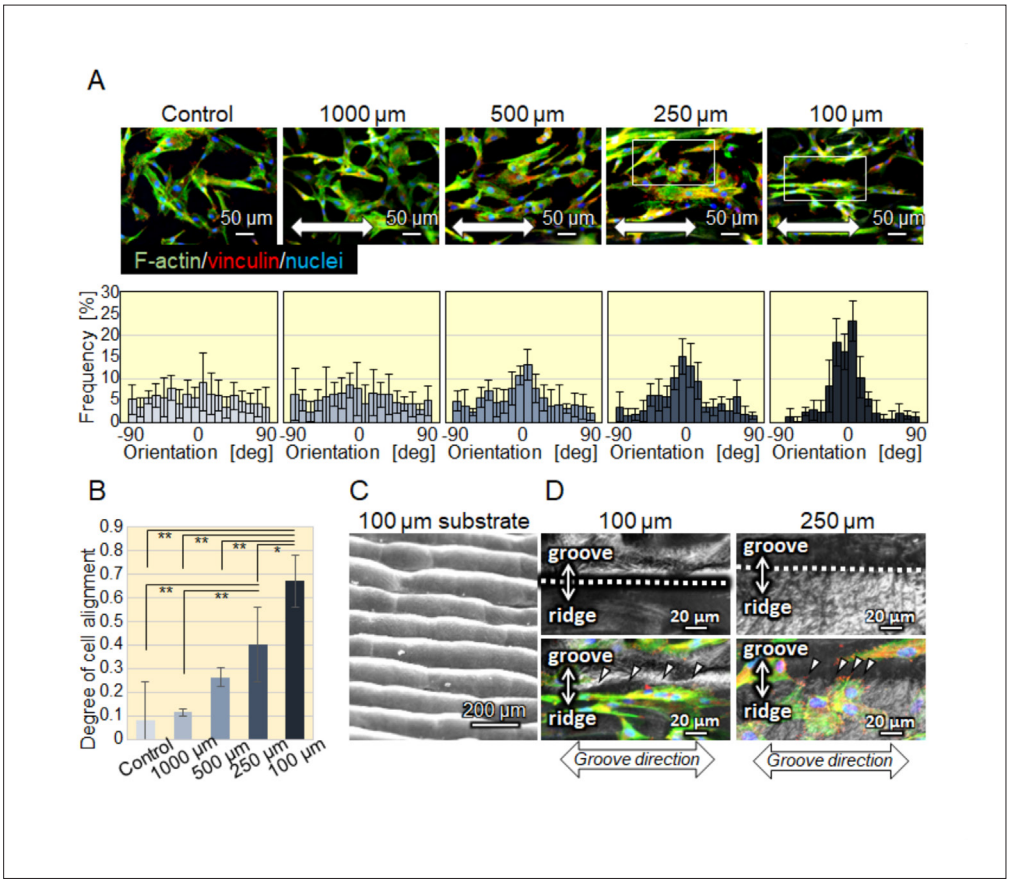

Figure 2. hMSCs alignment along the grooved structure. (A) Immunocytochemical images of hMSCs (upper side) and the corresponding angular distribution of the hMSCs. (B) The comparison of the degree of cell alignment in response to the groove size. *$p < 0.05$, **$p < 0.01$. (C) The magnified images of the 100 μm groove substrate. (D) The magnified images of 250 μm and 100 μm grooves as presented in (A), which show the focal adhesion accumulation at the interface between the groove and ridge.

3.4. Bone matrix orientation in long-term culture

After 4 weeks of long-term culture, MSCs produced type I collagen without any osteogenic stimuli and initiated early osteogenesis. Immunostaining images of the cells on 100 μm grooves surface demonstrated cell alignment as well as the preferred alignment of the collagen matrix along the groove direction (Figure 4).

4. Discussion

Targeted activation of stem cell fate using engineered materials is important for advancing tissue engineering and understanding stem cell biology. We report that the periodic surface structure induces osteogenic differentiation of MSCs associated with unidirectional cellular alignment. The surface topography was obtained using PBF-LB (Figure 1), which resulted in an optimal surface groove structure for guiding cell orientation. MSCs recognized the groove structure well, leading to unidirectional cellular arrangement (Figures 2A and B). The cells had the highest alignment along the patterns, with a width of 100 μm, which is relevant to the size of the elongated cells. The additive manufacturing topography showed a characteristic morphology with continuous roughness derived from the powders. The interaction between MSCs and the material surface was mediated by focal adhesion accumulation along the groove–ridge interface, resulting in unidirectional stress fiber alignment (Figure 2C). The cellular responses against the scaffold surface structure have been well recognized, but how the cells sense the attached materials and reorganize the cytoskeletal components is not yet fully understood.[27,28] It is important to understand the mechanisms favoring the grooved structural size. Microroughness can affect cellular activities by directly stimulating the cell membrane structure and cytoskeletal bending forces,[29,30] resulting in cell morphological alterations. Although the cellular alignment responses against nanometer-scale grooves are the same as in the case of microgrooves, the bone matrix alignment on nanogrooves shows quite a unique organization orthogonal to the cell alignment.

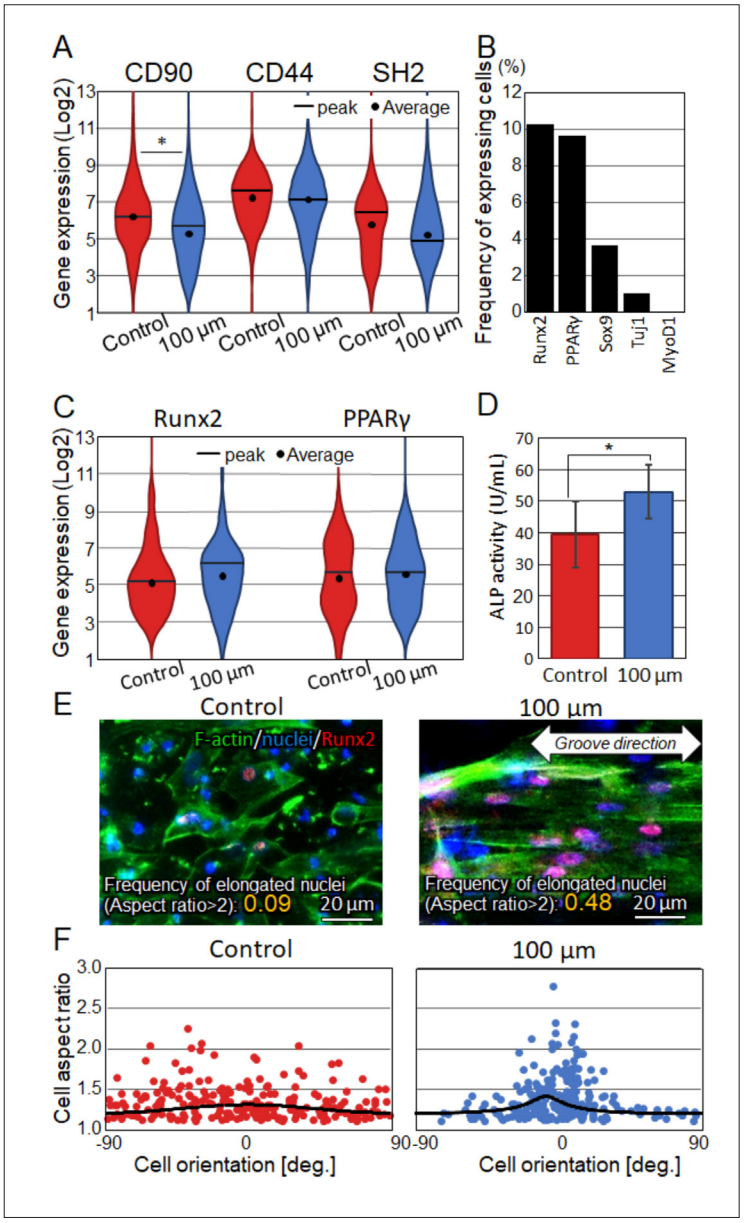

Figure 3. Osteogenic differentiation of hMSCs on 100 μm grooves. (A) Violin plot of the distribution of cells expressing *CD90*. *$p < 0.05$. (B) Comparison of the frequency of the lineage-specific gene-expressing cells on 100 μm grooves. (C) Comparison of *Runx2* and *PPARγ* expression between control and 100 μm grooves. (D) Comparison of the ALP activity between control and 100 μm grooves. (E) The immunocytochemical images of *Runx2* expression. (F) Cellular deformation analysis which shows the relationship between cellular orientation and aspect ratio.

This phenomenon is mediated by the maturation of focal adhesions connected to the cell-secreted collagen matrix.[23]

Gene sequencing analysis revealed that *CD90*, which maintains the stemness of MSCs, was significantly reduced in the grooved substrate, indicating that the grooved structure genetically facilitated the stem cell fate decision (Figure 3A). MSCs cultured on the grooves showed a specific commitment to the adipose/bone lineage (Figure 3B). Moreover, the cells favored osteogenic lineage rather than adipogenesis (Figure 3C). The cells on the microgroove surface showed significantly higher level of ALP activity rather than those on control surface (Figure 3D). This is possibly due to the nuclear deformation in aligned cells associated with mechanical switching (Figure 3E). The relationship between intrinsic mechanical cues and MSCs differentiation has been demonstrated.[31] Matrix or substrate stiffness has been shown to play an important role

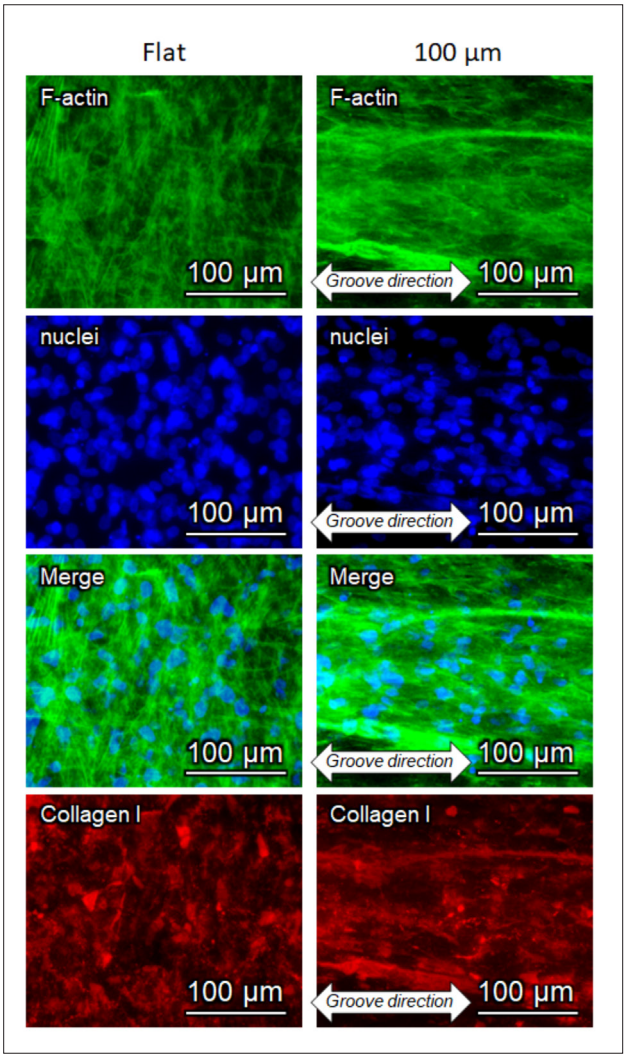

Figure 4. Type I collagen expression on control and 100 μm groove substrates. Notes: green, F-actin; red, type I collagen; blue, nuclei.

in regulating the differentiation of MSCs toward specific lineages.[5,6] In particular, cell shape has been shown to control adipogenic/osteogenic lineage commitment via the Rho/ROCK pathways,[32] which is consistent with our results. We found that the aligned MSCs, in response to the additive-manufactured groove structure, produced a type I collagen matrix even without any osteogenic differentiation stimuli (Figure 4), indicating osteogenic lineage commitment. The grooved structure possibly induced cellular tension along the patterning, which resulted in the deformation of nuclei and subsequent activation of some transcriptional factors.[33,34] We also succeeded in guiding the oriented bone-mimetic extracellular matrix microstructure from MSCs on a grooved substrate. Our previous findings demonstrated that unidirectional cellular alignment is key to functional bone regeneration.[16-18] This study revealed that hMSCs alignment has great osteogenic potency, as well as functional microstructural development (Figure 5).

PBF-LB, a type of metal additive manufacturing, enables the desired control of surface structure by melting and solidifying the metal powders based on CAD data. This technology can achieve complicated internal and external morphology and porosity control of the structure, all of which are hard to accomplish using conventional casting and cutting methods. It is also possible to control the crystallographic texture by optimizing the heat-source scanning strategy, which enables physical property control based on the orientation dependence of mechanical properties, such as Young's modulus, leading to the development of implants that can suppress harmful stress shielding.[35] It has been reported that the structural surface shape control by additive manufacturing induced osteoblast proliferation[36] and extracellular matrix

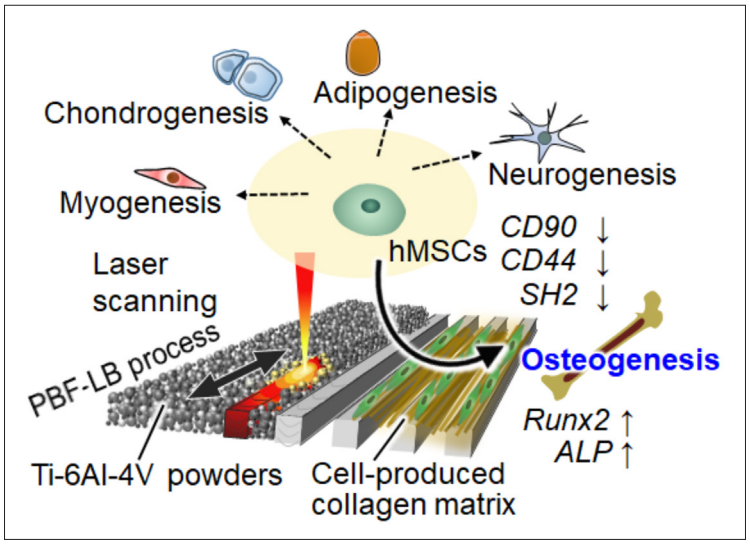

Figure 5. Schematic illustration of the findings. Metal additive-manufactured groove structures induced osteogenic differentiation of hMSCs, as well as the organization of aligned bone matrix, which is the determinant cue for bone mechanical functions.

secretion.[37] Furthermore, recent findings indicate that the building direction and scanning parameters also control the proliferation and gene expression of stem cells.[38,39] There is increasing evidence that the microstructure developed by additive manufacturing technology can control the cell morphology and possibly regulate their differentiation fate. Three-dimensional printing of porous titanium stimulated hMSCs proliferation and osteogenic differentiation.[40] They conclude that the increased number of cells on the microgroove surface possibly triggered osteogenic differentiation. Shen *et al.* modified surface using a laser metal deposition technique.[41] In addition, Wang *et al.* reported surface microgrooved Ti-6Al-4V alloys with graphene oxide coating fabricated by laser processing technique demonstrated osteogenic ability, and the optimal groove width size was 45 μm.[42] Moreover, metal composition has been reported to have an advantage for osteogenic lineage induction.[43] Our findings indicate that the microgroove Ti-6Al-4V surface has a significant advantage for osteogenic lineage induction, which is a promising factor for controlling hMSCs differentiation. The relationship between histone modification associated with nuclear deformation and the differentiation commitment is under investigation and will be reported in our future research. Considering shape control in PBF-LB depends on the powder size of the starting materials, the structural resolution of the obtained materials has some limitations. In this study, we determined 100 μm width as the smallest realizable size and investigated the effects of microgrooves on hMSCs properties ranging from 100 μm to 1000 μm. The optimal width of 100 μm grooves for osteogenesis control is consistent with our *in vivo* animal study. We have developed a vertebral fusion cage device that can induce excellent bone fusion without performing treatments, such as a large amount of autologous bone, using PBF-LB technology.[24,25] Additive manufacturing of biomedical devices is of great clinical importance in the case of spinal fusion spacers. Our findings shed light on a next-generation device for medical use that can realize tissue repair at the desired time.

5. Conclusion

It has been previously recognized that the biophysical properties of materials can affect stem cell fate; however, efficient strategies for osteogenic differentiation have not been established. This study revealed that metal additive-manufactured groove structures induced osteogenic differentiation of hMSCs, as well as aligned bone matrix organization, which is the determinant cue for bone mechanical functions. Our results present a novel platform for understanding the regulatory systems of stem cell lineages and therapeutic applications of stem cell regulators.

Acknowledgments

None.

Funding

This research was funded by JST, CREST, JPMJCR22L5, JPMJCR2194, Japan, and JSPS KAKENHI (grant numbers JP21H05197, JP20H003080, and JP18H05254).

Conflict of interest

The authors declare no conflicts of interest.

Author contributions

Conceptualization: Aira Matsugaki, Takayoshi Nakano
Investigation: Aira Matsugaki, Toko Mori, Mitsuka Saito, Kazuma Funaoku, Riku Yamano, Tadaaki Matsuzaka, Ryosuke Ozasa, Takayoshi Nakano
Methodology: Aira Matsugaki, Ozkan Gokcekaya, Takayoshi Nakano
Formal analysis: Toko Mori, Mitsuka Saito, Kazuma Funaoku, Riku Yamano, Tadaaki Matsuzaka, Ozkan Gokcekaya
Writing – original draft: Aira Matsugaki
Writing – review & editing: Takayoshi Nakano

Ethics approval and consent to participate

Not applicable.

Consent for publication

Not applicable.

Availability of data

The data presented in this study are available upon reasonable request from the corresponding author.

References

1. Pittenger MF, Discher DE, Péault BM, Phinney DG, Hare JM, Caplan AI. Mesenchymal stem cell perspective: cell biology to clinical progress. *NPJ Regen Med*. 2019;4(1):22. doi: 10.1038/s41536-019-0083-6
2. Grotheer V, Skrynecki N, Oezel L, Windolf J, Grassmann J. Osteogenic differentiation of human mesenchymal stromal cells and fibroblasts differs depending on tissue origin and replicative senescence. *Sci Rep*. 2021;11(1):11968. doi: 10.1038/s41598-021-91501-y
3. Mazzoni E, Mazziotta C, Iaquinta MR, et al. Enhanced osteogenic differentiation of human bone marrow-derived mesenchymal stem cells by a hybrid hydroxylapatite/collagen scaffold. *Front Cell Dev Biol.* 2021;8:610570. doi: 10.3389/fcell.2020.610570
4. Murphy W, McDevitt T, Engler AJ. Materials as stem cell regulators. *Nat Mater.* 2014;13(6):547-557. doi: 10.1038/nmat3937
5. Engler AJ, Sen S, Sweeney HL, Discher DE. Matrix elasticity directs stem cell lineage specification. *Cell.* 2006;126(4):677-689. doi: 10.1016/j.cell.2006.06.044
6. Park JS, Chu JS, Tsou AD, et al. The effect of matrix stiffness on the differentiation of mesenchymal stem cells in response to TGF-β. *Biomaterials.* 2011;32(16):3921-3930. doi: 10.1016/j.biomaterials.2011.02.019
7. McMurray RJ, Gadegaard N, Tsimbouri PM, et al. Nanoscale surfaces for the long-term maintenance of mesenchymal stem cell phenotype and multipotency. *Nat Mater*. 2011;10(8):637-644. doi: 10.1038/nmat3058
8. Dalby MJ, Gadegaard N, Tare T, et al. The control of human mesenchymal cell differentiation using nanoscale symmetry and disorder. *Nat Mater*. 2007;6(12):997-1003. doi: 10.1038/nmat2013
9. Barradas AM, Fernandes HA, Groen N, et al. A calcium-induced signaling cascade leading to osteogenic differentiation of human bone marrow-derived mesenchymal stromal cells. *Biomaterials*. 2012;33(11):3205-3215. doi: 10.1016/j.biomaterials.2012.01.020
10. Yang F, Yong D, Tu J, Zheng Q, Cai L, Wang L. Strontium enhances osteogenic differentiation of mesenchymal stem cells and in vivo bone formation by activating Wnt/catenin signaling. *Stem Cells.* 2011;29(6):981-991. doi: 10.1002/stem.646
11. Jayasree A, Raveendran NT, Guo T, Ivanovski S, Gulati K. Electrochemically nano-engineered titanium: Influence of dual micro-nanotopography of anisotropic nanopores on bioactivity and antimicrobial activity. *Mater Today Adv*. 2022;15:100256. doi: 10.1016/j.mtadv.2022.100256
12. Luo J, Walker M, Xiao Y, Donnelly H, Dalby MJ, Salmeron-Sanchez M. The influence of nanotopography on cell behaviour through interactions with the extracellular matrix – A review. *Bioact Mater*. 2022. 15:145-159. doi: 10.1016/j.bioactmat.2021.11.024
13. Matsugaki A, Aramoto G, Ninomiya T, et al. Abnormal arrangement of a collagen/apatite extracellular matrix orthogonal to osteoblast alignment is constructed by a nanoscale periodic surface structure. *Biomaterials.* 2015. 37:134-143. doi: 10.1016/j.biomaterials.2014.10.025
14. Frazier WE. Metal additive manufacturing: A review. *J Mater Eng Perform*. 2014;23(6):1917-1928. doi: 10.1007/s11665-014-0958-z
15. Hagihara K, Nakano T. Control of anisotropic crystallographic texture in powder bed fusion additive manufacturing of metals and ceramics - A review. *J Metals*. 2022.74(4):1760-1773. doi: 10.1007/s11837-021-04966-7
16. Matsugaki A, Aramoto G, Nakano T. The alignment of MC3T3-E1 osteoblasts on steps of slip traces introduced by dislocation motion. *Biomaterials*. 2012;33(30):7327-7335. doi: 10.1016/j.biomaterials.2012.06.022
17. Matsugaki A, Isobe Y, Saku T, Nakano T. Quantitative regulation of bone-mimetic, oriented collagen/apatite matrix structure depends on the degree of osteoblast alignment on oriented collagen substrates. *J Biomed Mater Res A*. 2015;103(2):489-499. doi: 10.1002/jbm.a.35189

18. Matsugaki A, Fujiwara N, Nakano T. Continuous cyclic stretch induces osteoblast alignment and formation of anisotropic collagen fiber matrix. *Acta Biomater*. 2013;9(7):7227-7235. doi: 10.1016/j.actbio.2013.03.015

19. Ozasa R, Matsugaki A, Matsuzaka T, Ishimoto T, Yun H-S, Nakano T. Superior alignment of human iPSC-osteoblasts associated with focal adhesion formation stimulated by oriented collagen scaffold. *Int J Mol Sci*. 2021;22(12):1-11. doi: 10.3390/ijms22126232

20. Nakano T, Kaibara K, Ishimoto T, Tabata Y, Umakoshi Y. Biological apatite (BAp) crystallographic orientation and texture as a new index for assessing the microstructure and function of bone regenerated by tissue engineering. *Bone*. 2012;51(4):741-747. doi: 10.1016/j.bone.2012.07.003

21. Nakano T, Kaibara K, Tabata Y, et al. Unique alignment and texture of biological apatite crystallites in typical calcified tissues analyzed by microbeam X-ray diffractometer system. *Bone*. 2002;31(4):479-487. doi: 10.1016/s8756-3282(02)00850-5

22. Ishimoto T, Nakano T, Umakoshi Y, Yamamoto M, Tabata Y. Degree of biological apatite c-axis orientation rather than bone mineral density controls mechanical function in bone regenerated using recombinant bone morphogenetic protein-2. *J Bone Miner Res*. 2013;28(5):1170-1179. doi: 10.1002/jbmr.1825

23. Nakanishi Y, Matsugaki A, Kawahara K, Ninomiya T, Sawada H, Nakano T. Unique arrangement of bone matrix orthogonal to osteoblast alignment controlled by Tspan11-mediated focal adhesion assembly. *Biomaterials*. 2019;209:103-110. doi: 10.1016/j.biomaterials.2019.04.016

24. Ishimoto T, Kobayashi Y, Takahata M, et al. Outstanding in vivo mechanical integrity of additively manufactured spinal cages with a novel "honeycomb tree structure" design via guiding bone matrix orientation. *Spine J*. 2022;22(10):1742-1757. doi: 10.1016/j.spinee.2022.05.006

25. Matsugaki A, Ito M, Kobayashi Y, et al. Innovative design of bone quality-targeted intervertebral spacer: Accelerated functional fusion guiding oriented collagen/apatite microstructure without autologous bone graft. *Spine J*. 2022;23(4):609-620. doi: 10.1016/j.spinee.2022.12.011

26. Kimura Y, Matsugaki A, Sekita A, Nakano T. Alteration of osteoblast arrangement via direct attack by cancer cells: New insights into bone metastasis. *Sci Rep*. 2017;7(1):1-11. doi: 10.1038/srep44824

27. Leclech C, Villard C. Cellular and subcellular contact guidance on microfabricated substrates. *Front Bioeng Biotechnol*. 2020;8:551505. doi: 10.3389/fbioe.2020.551505

28. Ramirez-San Juan GR, Gardel PW, Oakes ML. Contact guidance requires spatial control of leading-edge protrusion. Mol Biol Cell. 2017;28(8):1043-1053.

29. Bade ND, Kamien RD, Assoian RK, et al. Curvature and Rho activation differentially control the alignment of cells and stress fibers. *Sci Adv*. 2017;3(9):e1700150. doi: 10.1126/sciadv.1700150

30. Reynolds MJ, Hachicho C, Carl AG, Gong R, Alushin GM. Bending forces and nucleotide state jointly regulate F-actin structure. *Nature*. 2022;611(7935):380-386. doi: 10.1038/s41586-022-05366-w

31. Steward AJ, Kelly DJ. Mechanical regulation of mesenchymal stem cell differentiation. *J Anat*. 2015;227(6):717-731. doi: 10.1111/joa.12243

32. McBeath R, Pirone DM, Nelson CM, Bhadriraju K, Chen CS. Cell shape, cytoskeletal tension, and RhoA regulate stem cell lineage commitment. *Dev Cell*. 2004;6(4):483-495. doi: 10.1016/s1534-5807(04)00075-9

33. Pajerowski JD, Dahl KN, Zhong FL, et al. Physical plasticity of the nucleus in stem cell differentiation. *Proc Natl Acad Sci USA*. 2007;104(40):15619-15624. doi: 10.1073/pnas.0702576104

34. Swift J, Ivanovska IL, Buxboim A, et al. Nuclear lamin-A scales with tissue stiffness and enhances matrix-directed differentiation. *Science*. 2013;341(6149):1240104. doi: 10.1126/science.1240104

35. Gokcekaya O, Ishimoto T, Nishikawa Y, et al. Novel single crystalline-like non-equiatomic TiZrHfNbTaMo bio-high entropy alloy (BioHEA) developed by laser powder bed fusion. *Mater Res Lett*. 2023;11(4):274-280. doi: 10.1080/21663831.2022.2147406

36. Warnke PH, Douglas T, Wollny P, et al. Rapid prototyping: Porous titanium alloy scaffolds produced by selective laser melting for bone tissue engineering. *Tissue Eng C*. 2009;15(2):115-124. doi: 10.1089/ten.tec.2008.0288

37. Hrabe NW, Heinl P, Bordia RK, Körner Carolin, Fernandes RJ. Maintenance of a bone collagen phenotype by osteoblast-like cells in 3D periodic porous titanium (Ti-6Al-4V) structures fabricated by selective electron beam melting. *Connect Tissue Res*. 2013;54(6):351-360. doi: 10.3109/03008207.2013.822864

38. Wysocki B, Idaszek J, Zdunek J, et al. The influence of selective laser melting (SLM) process parameters on in-vitro cell response. *Int J Mol Sci*. 2018;19(6):1619. doi: 10.3390/ijms19061619

39. Weißmann V, Drescher P, Seitz H, et al. Effects of build orientation on surface morphology and bone cell activity of additively manufactured Ti6Al4V specimens. *Materials*. 2018;11(6):915. doi: 10.3390/ma11060915

40. Papaefstathiou S, Larochette N, Liste RMV, et al. Three-dimensional printing of biomimetic titanium mimicking trabecular bone induces human mesenchymal stem cell proliferation: An in-vitro analysis. *Spine*. 2022;47(14):1027. doi: 10.1097/brs.0000000000004317

41. Shen H, Liao C, Zhou J, Zhao K. Two-step laser based surface treatments of laser metal deposition manufactured Ti6Al4V components. *J Manuf Process.* 2021;64: 239-252. doi: 10.1016/j.jmapro.2021.01.028

42. Wang C, Hu H, Li Z, et al. Enhanced osseointegration of titanium alloy implants with laser microgrooved surfaces and graphene oxide coating. *ACS Appl Mater Interfaces*. 2019;11(43):39470-39483. doi: 10.1021/acsami.9b12733

43. Ninomiya JT, Struve JA, Krolikowski J, Hawkins Michael, Weihrauch D. Porous ongrowth surfaces alter osteoblast maturation and mineralization. *J Biomed Mater Res A*. 2015;103(1):276-281. doi: 10.1002/jbm.a.35140